IOP Publishing Physics in Medicine and Biology

Phys. Med. Biol. **52** (2007) 6923–6930 doi:10.1088/0031-9155/52/23/010

High-resolution brain tumor visualization using three-dimensional x-ray phase contrast tomography

F Pfeiffer[1,2], O Bunk[1], C David[1], M Bech[3], G Le Duc[4], A Bravin[4] and P Cloetens[4]

[1] Paul Scherrer Institut, CH-5232 Villigen PSI, Switzerland
[2] Ecole Polytechnique Fédérale de Lausanne, CH-1015 Lausanne, Switzerland
[3] Niels Bohr Institute, University of Copenhagen, DK-2100 Copenhagen, Denmark
[4] European Synchrotron Radiation Facility, B.P. 220, 38043 Grenoble Cedex, France

E-mail: franz.pfeiffer@psi.ch

Received 6 August 2007, in final form 15 October 2007
Published 8 November 2007
Online at stacks.iop.org/PMB/52/6923

Abstract

We report on significant advances and new results concerning a recently developed method for grating-based hard x-ray phase tomography. We demonstrate how the soft tissue sensitivity of the technique is increased and show *in vitro* tomographic images of a tumor bearing rat brain sample, without use of contrast agents. In particular, we observe that the brain tumor and the white and gray brain matter structure in a rat's cerebellum are clearly resolved. The results are potentially interesting from a clinical point of view, since a similar approach using three transmission gratings can be implemented with more readily available x-ray sources, such as standard x-ray tubes. Moreover, the results open the way to *in vivo* experiments in the near future.

(Some figures in this article are in colour only in the electronic version)

1. Introduction

Phase-sensitive x-ray imaging, which uses the phase shift rather than the absorption as the imaging signal has the potential of substantially increased contrast in biological samples (Fitzgerald 2000, Momose 2005). Various phase-sensitive x-ray imaging methods were developed in the past years. They can be classified into interferometric methods (Bonse and Hart 1965, Momose *et al* 2003, Weitkamp *et al* 2005), techniques using an analyzer (Davis *et al* 1995, Ingal and Beliaevskaya 1995, Chapman *et al* 1997), and free-space propagation methods (Snigirev *et al* 1995, Nugent *et al* 1996, Wilkins *et al* 1996). Some of the methods not only generate a form of phase contrast, but also provide quantitative phase information, which can be used for advanced image analysis. The extension to computed tomography (CT) is one such interesting possibility providing three-dimensional information about the specimen (Momose *et al* 1996, Beckmann *et al* 1997, Cloetens *et al* 1999, McMahon *et al* 2003, 2006, Groso *et al* 2006, Pfeiffer *et al* 2007a).

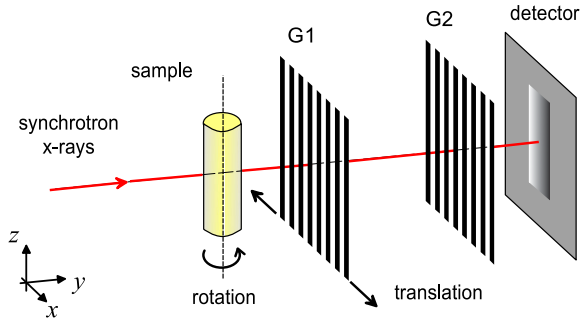

Figure 1. Schematic of the setup for x-ray phase tomography using a grating interferometer. For each projection a series of at least four images is recorded while one of the gratings (G1) is scanned along the *x*-direction.

In this paper we report on significant advances of a recently developed method for grating-based hard x-ray phase tomography (Weitkamp *et al* 2005, Momose *et al* 2006). More precisely, we describe the combination of three particular improvements concerning (i) the application of gratings with higher contrast made by a novel fabrication process, (ii) a high precision and high speed setup for the phase stepping procedure and (iii) the application of an improved tomographic phase reconstruction algorithm.

2. Materials and methods

2.1. Experimental setup

The principles of differential phase contrast imaging using a grating interferometer have been described in detail in Weitkamp *et al* (2005), Momose *et al* (2006), Pfeiffer *et al* (2006a), and are only briefly reviewed here. Figure 1 shows our experimental arrangement. It consists of the specimen on a rotation stage, a phase grating G1 and an analyzer absorption grating G2. The first grating (G1) acts as phase mask, and imprints periodic phase modulations onto the x-ray wave front. Through the Talbot effect, the phase modulation is transformed into an intensity modulation in the plane of the second grating (G2), forming a linear periodic fringe pattern perpendicular to the optical axis and parallel to the lines of G1 (Momose *et al* 2006, Weitkamp *et al* 2007). The second grating (G2) with absorbing lines and the same periodicity and orientation as the fringes created by G1 is placed in the detection plane, immediately in front of the detector. When one of the gratings is scanned along the transverse direction ('phase stepping'), the intensity signal in each pixel in the detector plane oscillates as a function of the grating position. The fundamental idea of the method is to analyze, for each pixel, the changes of these oscillations, when an object is placed into the x-ray beam. As described in more detail in Weitkamp *et al* (2005), Pfeiffer *et al* (2006a), a single phase-stepping scan (a series of at least four images taken at different positions of the scanned grating) yields both quantitative images of the specimen's phase shift gradient, $\mathrm{d}\Phi(x, z)/\mathrm{d}x$, and the conventional transmission projection.

Three-dimensional (3D) information of the specimen using computed tomography (CT) can be obtained, when the specimen is rotated around the rotation axis and a phase stepping series is recorded for each angle. The tomography data set can be reconstructed by integrating the pre-processed differential phase contrast projection images line by line and then performing

a standard tomographic reconstruction (Weitkamp *et al* 2005). A method that not only saves computing time but also generally yields better reconstructions is to directly reconstruct the 3D volume data set from the pre-processed differential phase contrast projections by using a modified filter kernel (Hilbert transform) in the FBP reconstruction (see Pfeiffer *et al* (2007a), (2007b), Faris and Byer (1988) for a more detailed description). The latter approach was used for the present study. The reconstructed quantity is the real part of the x-ray refractive index (as opposed to standard absorption-contrast tomography, where it is the absorption coefficient).

2.2. Image acquisition

The imaging experiments were carried out at the beamline ID19 while the tumor implantation was performed at the BioMedical Facility of the European Synchrotron Radiation Facility (ESRF, Grenoble). A monochromatic x-ray beam of 24.9 keV ($\lambda = 0.498$ Å) was used for the measurements. The interferometer was placed at a distance of 140 m from the wiggler source. The gratings were fabricated by a process involving photolithography, deep etching into silicon and electroplating of gold. The first grating (Si phase grating, G1) had a period of $p_1 = 3.99$ μm and a height of $h_1 = 31.7$ μm. The corresponding values for the second grating (gold absorber grating, G2) were $p_2 = 2.00$ μm and $h_2 = 30$ μm. In contrast to the earlier experiments (Weitkamp *et al* 2005), a novel grating fabrication protocol was used (David *et al* 2007). This allowed the fabrication of unprecedentedly high aspect ratios (60:1) for the absorbing lines of the analyzer grating (G2), thus increasing the contrast of the intensity modulation recorded during a phase-stepping scan. The field-of-view was matched to the size of the specimen (rat brain) and was 16.1× 16.1 mm^2. To achieve a very high angular, and thus phase sensitivity, the distance between G1 and G2 was chosen to be as large as 361 mm (ninth fractional Talbot distance (Weitkamp *et al* 2007)). The images were recorded using a 15 μm thick polycrystalline gadolinium oxysulfide scintillation screen with a magnifying optical lens system and a cooled charge coupled device (CCD). We used the FReLoN 2000 (a fast-readout, low-noise CCD developed at the ESRF) with 1024 × 1024 pixels and a 28.0 × 28.0 μm^2 pixel size (in the 2 × 2 binning mode). Due to the magnifying lens system, the effective pixel size in the recorded images was 15.7 × 15.7 μm^2.

For the acquisition of a full tomographic data set, the object was rotated around the tomographic rotation axis and images were recorded for each projection angle. To both increase the positioning accuracy of the grating during the phase stepping scan and to decrease the overhead time due to motor movements, a piezo-driven translation stage with an active feedback loop was used for this experiment. The latter consisted of a PI Hera piezo nano-positioning system (P-621.1CL) with the corresponding analog amplifier in a closed loop operation with a positioning accuracy of <10 nm. A detailed analysis (standard deviation) of the background regions in the differential phase contrast projection images showed that due to the high positioning accuracy of the piezo stage an angular sensitivity of 0.014 μrad could be obtained in the measured data. Furthermore, this configuration enabled us to acquire a whole data set of 721 projections, each consisting of eight images, within a total exposure time of less than 40 min (0.4 s exposure time per individual image). This proved to be of crucial importance to achieve a high sensitivity, because it suppresses artifacts in the data, which are otherwise unavoidable due to long term drifts or instabilities of the mechanical setup, the monochromator or the synchrotron beam itself. Note that the total exposure time can potentially be reduced to below 10 min for future *in vivo* experiments by reducing both the number of tomographic projections and the exposure time for each individual image by 50% without significantly compromising on the spatial resolution and sensitivity in the reconstructed 3D images.

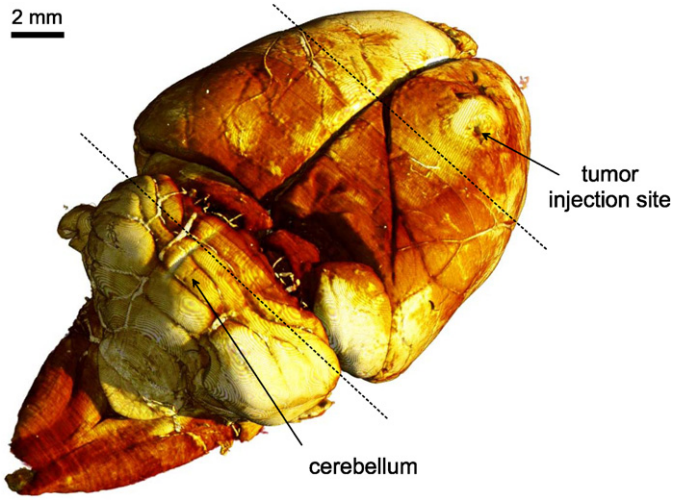

Figure 2. Post mortem three-dimensional image obtained on a rat brain bearing a 9 L gliosarcoma. The volume data set was reconstructed from 721 high sensitivity differential phase contrast projections measured at a synchrotron x-ray source.

2.3. Sample preparation

The rat brain specimen was prepared according to the following details.

Cell line: the 9 L gliosarcoma cell line (Coderre *et al* 1994) was established by (Benda *et al* 1971). Cells were grown as monolayers with Dulbecco's Modified Eagle Medium (DMEM) (Gibco-Invitrogen, France; Cergy-Pontoise, France) without sodium pyruvate (with 4500 mg l^{-1} of glucose and pyridoxine HCl) supplemented with 10% fetal calf serum, 0.2% penicillin/streptomycin and incubated at 37 °C in a mixture of air-CO_2 (95%–5%).

Tumor implantation: the male Fisher 344 rats (180–280 g, Charles River, L' Arbresle, France) were placed on a stereotactic head holder (model 900, David Kopf Instruments, Tujunga, USA). The tumor cells were injected at D0 as described previously (Kobayashi *et al* 1980). Before injection in the brain, 10^4 cells were suspended into 1 μl DMEM with antibiotics (1%) manually injected using a 1 μl Hamilton syringe through a burr hole in the right caudate nucleus (7.5 mm anterior to the ear bars, 3.5 mm lateral to the midline and 5.5 mm depth from the skull) (Paxinos and Watson 1986). The burr hole was plugged and the scalp sutured. All operative procedures related to animal care strictly conformed to the Guidelines of the French Government (licenses 380324/380456 and A3818510002) and were reviewed by the Comité d'Ethique Régional Rhône-Alpes.

3. Results and discussion

For an overview, figure 2 shows a three-dimensional rendering of the reconstructed volume data set. The reconstructed quantity that is displayed is the real part of the x-ray refractive index.

Figures 3 and 4 show slices through the specimen, revealing two interesting findings. The first observation, supported by what can be seen in the tomographic image slice through the brain region containing the rat's *cerebellum* (figure 3(a)), concerns the contrast between the brain's white and gray matter. Although such differentiation is usually hardly possible based

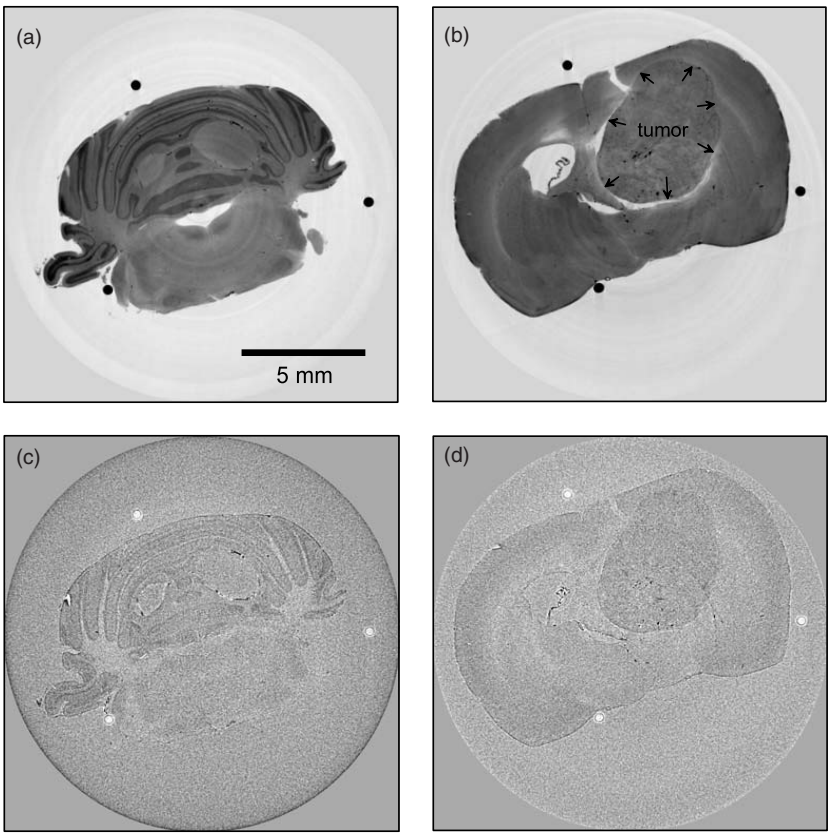

Figure 3. Phase and attenuation-based tomography results. (a) Phase tomography slice through the rat's cerebellum showing a clear contrast between the white and gray brain matter. (b) Slice through a region of the brain containing a tumor (arrows indicate the tumor's 'pushing front', the border between the tumor-invaded and healthy brain tissue). (c) and (d) Corresponding slices through the absorption-based reconstruction of the specimen. All images are displayed on a linear gray scale corresponding to $\pm 2\sigma$, where σ is the standard deviation of the pixel gray values in the image.

on x-ray CT scans, our method clearly resolves these small density differences in the brain tissue structure. Based on the standard deviation of the gray values in background (formalin) regions of the reconstructed tomographic slices, we deduce a measurement sensitivity for the real part of the refractive index of 2.0×10^{-10}. This corresponds to an electron density sensitivity of 0.18 e nm^{-3} and a mass density sensitivity of approximately 0.53 mg cm^{-3} for aqueous specimens. For comparison, a corresponding tomographic slice through the conventional absorption-based reconstruction is shown in figure 3(c). For the latter, we have averaged all frames recorded at each viewing angle to yield a non-interferometric projection image and used a standard absorption-based CT reconstruction protocol (Kak and Slaney 1987). Importantly, both results (figures 3(a) and (c)) have been obtained from the same data set, i.e., with the same exposure time.

The second observation, which confirms the enhanced tissue sensitivity of the method, is shown in figure 3(b). It displays a tomographic slice through a region in the brain which contains pathologic tissue, i.e. a brain tumor. Figure 3(b) shows clearly the presence of a 9 L gliosarcoma in the right caudate nucleus of the brain. Due to the presence of the tumor,

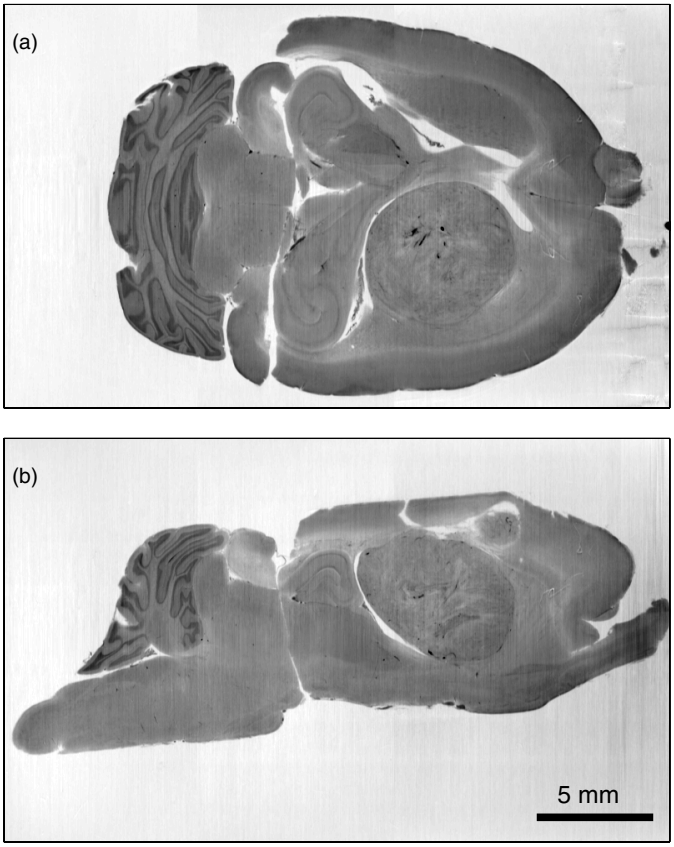

Figure 4. Additional slices through the phase tomography reconstruction: (a) frontal slice and (b) sagittal slice.

the midline is shifted and the left ventricule is dilated. The boundaries between the tumor and the healthy tissues are clearly defined. Moreover, the intra-tumoral heterogeneity can be seen with patches of various gray levels in the tumor itself. This probably corresponds to the presence of both necrotic and viable (with a high cellularity) areas as defined for that model (Henderson *et al* 1981). It has to be noted that our technique reveals the difference between corpus callosum and caudate nucleus.

Based on these results we conclude that both the differentiation of the white from the gray brain matter and details of the tumor invasion clearly demonstrate the potential of the method for biomedical studies, i.e. for high-resolution brain investigations. Since the spatial resolution of the presented results was mainly limited by the point spread function of the detection system, which typically is a factor of two larger than the effective pixel size, further improvements are easily possible in that respect. Increasing the resolution to a length scale corresponding to the second grating period (2 μm) is straightforward and can be achieved by changing the detector optics accordingly.

4. Summary

In summary, we have demonstrated how an improved grating-based phase contrast tomography setup yields images of biomedical specimens with unprecedented soft tissue sensitivity at

synchrotron x-ray sources. In particular we have shown that this x-ray method can be used to discern between subtle details of the tissue structure of animal brains, an application field which until now has almost exclusively been reserved for other, e.g. MRI, techniques. While the results can be applied immediately for biomedical studies at synchrotron x-ray sources, they are potentially interesting from a clinical point of view, since a similar approach can be implemented with more readily available x-ray sources, such as standard x-ray tubes (Pfeiffer *et al* 2007a, Pfeiffer *et al* 2006a).

Acknowledgments

We gratefully acknowledge J Bruder and C Grünzweig for the grating fabrication, C Kottler for help during the experiments and T Weitkamp for fruitful discussions. This work was supported by the European Synchrotron Radiation Facility (project MI-825) by allocation of beam time.

References

Beckmann F, Bonse U, Busch F and Gunnewig O J 1997 X-ray microtomography (mu CT) using phase contrast for the investigation of organic matter *J. Comput. Assist. Tomogr.* **21** 539–53

Benda P, Someda K, Messer J and Sweet W H 1971 Morphological and immunochemical studies of rat glial tumors and clonal strains propagated in culture *J. Neurosurg.* **34** 310–23

Bonse U and Hart M 1965 An x-ray interferometer *Appl. Phys. Lett.* **6** 155–6

Chapman L D, Thomlinson W C, Johnston R E, Washburn D, Pisano E, Gmuer N, Zhong Z, Menk R, Arfelli F and Sayers D 1997 Diffraction enhanced x-ray imaging *Phys. Med. Biol.* **42** 2015–25

Cloetens P, Ludwig W, Baruchel J, van Dyck D, van Landuyt J, Guigay J P and Schlenker M 1999 Holotomography: quantitative phase tomography with micrometer resolution using hard synchrotron radiation x rays *Appl. Phys. Lett.* **75** 2912–4

Coderre J A, Button T M, Micca P L, Fisher C D, Nawrocky M M and Liu H B 1994 Neutron-capture therapy of the 9 L rat gliosarcoma using the p-boronphenylalanine-fructose complex *Int. J. Radiat. Oncol. Biol. Phys.* **30** 643–52

David C, Bruder J, Rohbeck T, Grünzweig C, Kottler C, Diaz A, Bunk O and Pfeiffer F 2007 Fabrication of diffraction gratings for hard x-ray phase contrast imaging *Microelectron. Eng.* **84** 1172–7

Davis T J, Gao D, Gureyev T E, Stevenson A W and Wilkins S W 1995 Phase-contrast imaging of weakly absorbing materials using hard x-rays *Nature* **373** 595–8

Faris G W and Byer R L 1988 3-dimensional beam-deflection optical tomography of a supersonic jet *Appl. Opt.* **27** 5202–6

Fitzgerald R 2000 Phase-sensitive x-ray imaging *Phys. Today* **53** 23–7

Groso A, Stampanoni M, Abela R, Schneider P, Linga S and Müller R 2006 Phase contrast tomography: an alternative approach *Appl. Phys. Lett.* **88** 214104

Henderson S D, Kimler B F and Morantz R A 1981 Radiation-therapy of 9 L rat-brain tumors *Int. J. Radiat. Oncol. Biol. Phys.* **7** 497–502

Ingal V N and Beliaevskaya E A 1995 X-ray plane wave topography observation of the phase contrast from a noncrystalline object *J. Phys.* D **28** 2314–7

Kak A C and Slaney M 1987 *Principles of Computerized Tomography* (New York: IEEE Press)

Kobayashi N, Allen N, Clendenon N R and Ko L W 1980 An improved rat-brain tumor model *J. Neurosurg.* **53** 808–15

McMahon P J, Peele A G, Paterson D, Lin J J A, Irving T H K, McNulty I and Nugent K A 2003 Quantitative x-ray phase tomography with sub-micron resolution *Opt. Commun.* **217** 53–7

Momose A 2005 Recent advances in x-ray phase imaging *Japan. J. Appl. Phys.* **44** 6355–9

Momose A, Kawamoto S, Koyama I, Hamaishi Y, Takai K and Suzuki Y 2003 Demonstration of x-ray Talbot interferometry *Japan. J. Appl. Phys.* **42** 866–9

Momose A, Takeda T, Itai Y and Hirano K 1996 Phase-contrast x-ray computed tomography for observing biological soft tissues *Nat. Med.* **2** 473–5

Momose A, Yashiro W, Takeda Y, Suzuki Y and Hattori T 2006 Phase tomography by x-ray Talbot interferometry for biological imaging *Japan. J. Appl. Phys.* **45** 5254–62

Paxinos G and Watson C (ed) 1986 *The Rat Brain in Stereotaxic Coordinates* (New York: Academic)
Pfeiffer F, Grünzweig C, Bunk O, Frei G, Lehmann E and David C 2006a Neutron phase imaging and tomography *Phys. Rev. Lett.* **96** 215505
Pfeiffer F, Kottler C, Bunk O and David C 2007a Hard x-ray phase tomography with low-brilliance sources *Phys. Rev. Lett.* **98** 108105
Pfeiffer F, Kottler C, Bunk O and David C 2007b Tomographic reconstruction of three-dimensional objects from hard x-ray differential phase contrast projection images *Nucl. Instrum. Meth. Phys. Res.* A **580** 925–8
Pfeiffer F, Weitkamp T, Bunk O and David C 2006b Phase retrieval and differential phase-contrast imaging with low-brilliance x-ray sources *Nat. Phys.* **2** 258–61
Nugent K A, Gureyev T E, Cookson D F, Paganin D and Barnea Z 1996 *Phys. Rev. Lett.* **77** 2961–4
Snigirev A, Snigireva I, Kohn V, Kuznetsov S and Schelokov I 1995 On the possibilities of x-ray phase contrast microimaging by coherent high-energy synchrotron radiation *Rev. Sci. Instrum.* **66** 5486–92
Wilkins S W, Gureyev T E, Gao D, Pogany A and Stevenson A W 1996 Phase-contrast imaging using polychromatic hard x-rays *Nature* **384** 35–337
Weitkamp T, David C, Kottler C, Bunk O and Pfeiffer F 2007 Tomography with grating interferometers at low-brilliance sources *Proc. SPIE* **6318** 28–31
Weitkamp T, Diaz A, David C, Pfeiffer F, Stampanoni M, Cloetens P and Ziegler E 2005 X-ray phase imaging with a grating interferometer *Opt. Exp.* **13** 6296–304